

## Accepted Article

**Title:** Mass-production of Mesoporous MnCo<sub>2</sub>O<sub>4</sub> Spinel with MnIV- and CoII-rich Surface for Superior Bifunctional Oxygen Electrocatalysis

**Authors:** Wenhai Wang, Long Kuai, Wei Cao, Marko Huttula, Sami Ollikkala, Taru Ahopelto, Ari-Pekka Honkanen, Simo Huotari, Mengkang Yu, and Baoyou Geng

This manuscript has been accepted after peer review and appears as an Accepted Article online prior to editing, proofing, and formal publication of the final Version of Record (VoR). This work is currently citable by using the Digital Object Identifier (DOI) given below. The VoR will be published online in Early View as soon as possible and may be different to this Accepted Article as a result of editing. Readers should obtain the VoR from the journal website shown below when it is published to ensure accuracy of information. The authors are responsible for the content of this Accepted Article.

**To be cited as:** *Angew. Chem. Int. Ed.* 10.1002/anie.201708765  
*Angew. Chem.* 10.1002/ange.201708765

**Link to VoR:** <http://dx.doi.org/10.1002/anie.201708765>  
<http://dx.doi.org/10.1002/ange.201708765>

# Mass-production of Mesoporous $\text{MnCo}_2\text{O}_4$ Spinel with $\text{Mn}^{\text{IV}}$ - and $\text{Co}^{\text{II}}$ -rich Surface for Superior Bifunctional Oxygen Electrocatalysis

Wenhai Wang, Long Kuai, Wei Cao, Marko Huttula, Sami Ollikkala, Taru Ahopelto, Ari-Pekka Honkanen, Simo Huotari, Mengkang Yu, and Baoyou Geng\*

**Abstract:** A mesoporous  $\text{MnCo}_2\text{O}_4$  electrode materials is successfully fabricated for bifunctional oxygen electrocatalysis. The  $\text{MnCo}_2\text{O}_4$  exhibits both  $\text{Co}_3\text{O}_4$ -like activity for oxygen evolution reaction (OER) and  $\text{Mn}_2\text{O}_3$ -approaching performance for oxygen reduction reaction (ORR). The potential difference between ORR metric and OER metric of  $\text{MnCo}_2\text{O}_4$  is as low as 0.83 V. By XANES and XPS investigation, the notable activity is resulted from the preferred  $\text{Mn}^{\text{IV}}$ - and  $\text{Co}^{\text{II}}$ -rich surface. Valuably, the products can be obtained in large-scale with the precise chemical components at relatively low temperature. The surface state engineering maybe open a new avenue to optimize electrocatalysis performance of electrode materials. The prominent bifunctional activity shows that  $\text{MnCo}_2\text{O}_4$  has the possibility of being used in metal-air batteries and/or other energy devices.

Considerable interest has been focused on oxygen electrocatalysis for its important role in energy storage and conversion.<sup>[1]</sup> The Pt-based materials are regarded as the best catalysts toward ORR, but they are suffered from a poor OER activity.<sup>[2]</sup> There are a few catalysts possessing OER performance which can be comparable with Ir- or Ru-based materials.<sup>[3]</sup> Nevertheless, Ir- or Ru-based materials show a normal activity toward ORR. Although alloys of Pt, Ir and Ru have been used as bifunctional catalysts, their scarcity and high cost also hamper their applications.<sup>[4]</sup>

Among the developed bifunctional oxygen-catalysts<sup>[5]</sup>, heteroatoms doped carbon materials have been paid numerous attention because of heteroatoms doping can change the asymmetry spin density and the local charge density of carbon lattice<sup>[5c-e]</sup>. In order to perform the synergistic effects of heteroatoms, the synthesized temperatures of heteroatoms doped carbon materials

often beyond 800 °C but the precise doping is difficult to achieve.<sup>[5c,d]</sup> Contrastly, metal oxides are easily synthesized at lower temperatures. However, ordinary pure metal oxides with ideal crystal structure often exhibit single oxygen electrocatalysis activity of either OER or ORR. Various fabrication engineering has been developed to modulate the structure or component of metal oxides to motivate their bifunctional performance.<sup>[6]</sup> The structure or component engineering often involve some complicated processes and the yield is limited. Fortunately, previous researches have also revealed that the electrocatalytic activity has a great connection with the surface chemical state. Just as reported, average Mn valence locates in the region between  $\text{Mn}^{\text{III}}$  and  $\text{Mn}^{\text{IV}}$  can greatly improve the ORR activity of manganese oxides, in which the driving force comes from the  $e_g$  orbit number change from zero to one that can reduce oxygen adsorption and facilitate the exchange of hydroxyl by oxygen.<sup>[7]</sup> It is noticed that  $\text{MnCo}_2\text{O}_4$  is one of spinel oxides possess the structural flexibility and mixed valence states. Most of the reported  $\text{MnCo}_2\text{O}_4$  catalysts have a good activity toward OER, whereas the ORR activity is clumsy.<sup>[8]</sup> The main reason is that the average Mn valence of these  $\text{MnCo}_2\text{O}_4$  catalysts is between  $\text{Mn}^{\text{II}}$  and  $\text{Mn}^{\text{III}}$ , preventing ORR being improved. We are fortunate to have developed a facile spray-pyrolysis approach for the fabrication of mesoporous  $\text{Mn}_2\text{O}_3$  with Pt/C comparable ORR activity via modulating Mn chemical state.<sup>[9]</sup> Therefore, it is also expectable to achieve the bifunctional performance of  $\text{MnCo}_2\text{O}_4$  through surface chemical state engineering.

Herein, we reported a mesoporous  $\text{MnCo}_2\text{O}_4$  possess dominant  $\text{Mn}^{\text{IV}}$  in the surface and  $\text{Mn}^{\text{III}}$  in bulk while  $\text{Co}^{\text{II}}$  both in the surface and bulk, which exhibit high activity toward both ORR and OER with the potential difference between ORR and OER metrics of 0.83 V. The study of Zn-air batteries device shows that the initial discharge and charge potential of  $\text{MnCo}_2\text{O}_4$  are respectively 1.21 V and 2.05 V at the power density of 10 mA/cm<sup>2</sup>. After 180 cycles, there is only a small potential drop in discharge (1.10 V) and up in charge (2.32 V), which is superior to Pt/C in the same condition. Notably, the products can be synthesized in large-scale at a relatively low temperature.

The fabrication of the products is performed on the home-made equipment.<sup>[10]</sup> The SEM and TEM images (Figure 1a-b and Figure S1a-b, d-e) reveal that the obtained products are porous spheres with the size of 1-2  $\mu\text{m}$ , which is similar to that of  $\text{Mn}_2\text{O}_3$  and  $\text{Co}_3\text{O}_4$  prepared under same condition. The lattice fringe in HRTEM image (Figure 1c) is indexed to the (220) plane

[\*] Mr. W. H. Wang, Dr. L. Kuai, Mr. M. K. Yu, Prof. & Dr. B. Y. Geng  
College of Chemistry and Materials Science  
The Key Laboratory of Functional Molecular Solids, Ministry of Education, Anhui Laboratory of Molecular-Based Materials, Center for Nano Science and Technology, Anhui Normal University  
No.1 Beijing East Road, Wuhu, 241000, P. R. China.  
E-mail: [bygeng@mail.ahnu.edu.cn](mailto:bygeng@mail.ahnu.edu.cn)  
Dr. W. Cao, Dr. Prof. M. Huttula  
Nano and Molecular Systems Research Unit, University of Oulu,  
P.O. Box 3000, FIN-90014 Oulu, Finland  
Mr. S. Ollikkala, Mr. T. Ahopelto, Mr. A.-P. Honkanen, Prof. Simo Huotari  
Department of Physics, University of Helsinki, PO Box 64, FI-00014 Helsinki, Finland

## COMMUNICATION

WILEY-VCH

of  $\text{MnCo}_2\text{O}_4$ . The SEM element mapping (Figure 1d) proves the elements of Mn, Co and O distributing uniformly in the product. The powder X-ray diffraction (XRD) pattern (Figure 1e) confirms the phases of the samples can be assigned to  $\text{Mn}_2\text{O}_3$  (JCPDS 41-1442),  $\text{Co}_3\text{O}_4$  (JCPDS 74-1656) and  $\text{MnCo}_2\text{O}_4$  (JCPDS 77-0471). Compared to peaks of  $\text{Co}_3\text{O}_4$ , the peaks of  $\text{MnCo}_2\text{O}_4$  shift slightly to smaller angles. The substitution of larger size Mn cations results in the improvement of d (lattice fringe).<sup>[11]</sup>

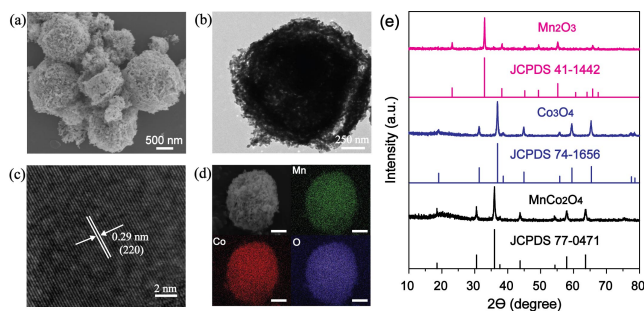


**Figure 1.** (a) SEM, (b) TEM, (c) HRTEM, (d) SEM element mapping (scale bars: 500 nm) images of  $\text{MnCo}_2\text{O}_4$ ; (e) XRD patterns of  $\text{MnCo}_2\text{O}_4$ ,  $\text{Co}_3\text{O}_4$  and  $\text{Mn}_2\text{O}_3$ .

The  $\text{N}_2$  adsorption-desorption curves in Figure S2a reveal that the surface areas of  $\text{MnCo}_2\text{O}_4$ ,  $\text{Mn}_2\text{O}_3$  and  $\text{Co}_3\text{O}_4$  are  $23.57 \text{ m}^2/\text{g}$ ,  $40.15 \text{ m}^2/\text{g}$  and  $19.28 \text{ m}^2/\text{g}$ , respectively. The  $\text{N}_2$  adsorption-desorption curves also show a loop occurs in the range of 0.9-1.0 P/P<sub>0</sub>. The mesoporous porous structure can promote the formation of active sites (Figure S2b), improving the electrochemistry activity of catalysts.

The X-ray photoelectron spectroscopy (XPS) was shown in Figure 2. In the Mn spectra (Figure 2a), the peaks at 644.2 eV and 654.7 eV are characteristic peaks of  $\text{Mn}^{\text{IV}}$ .<sup>[8a]</sup> The peaks at 641.3 eV and 653.3 eV are assigned to  $\text{Mn}^{\text{III}}$ .<sup>[8b]</sup> The peaks of 641.5 eV and 653.0 eV are ascribed to  $\text{Mn}^{\text{II}}$ .<sup>[8c]</sup> According to Figure 2a, the  $\text{Mn}2\text{p}_{3/2}$  and  $\text{Mn}2\text{p}_{1/2}$  for  $\text{MnCo}_2\text{O}_4$  shift to higher binding energy, showing the slightly higher surface Mn valence of  $\text{MnCo}_2\text{O}_4$  than  $\text{Mn}_2\text{O}_3$ . Apparently, the ratio of  $\text{Co}^{\text{II}}/\text{Co}^{\text{III}}$  for  $\text{MnCo}_2\text{O}_4$  is higher than  $\text{Co}_3\text{O}_4$  in Figure 2c. The calculated surface Co and Mn oxidation states of  $\text{MnCo}_2\text{O}_4$  from XPS were 2.47 and 3.19 (Table S1), which display the preferred state with  $\text{Mn}^{\text{IV}}$ - and  $\text{Co}^{\text{II}}$ -rich surface. Meanwhile, the Mn (Figure 2b) and Co (Figure 2d) K-edge x-ray absorption near edge structures (XANES) were further investigated its electron structure in bulk due to much larger detection depth. It is obvious that the Co's binding energy in  $\text{MnCo}_2\text{O}_4$  is less than  $\text{Co}_3\text{O}_4$  (insets of Figure 2d), which matches with the XPS results, suggesting that the  $\text{Co}^{\text{II}}$  is dominant type in the both surface and bulk of  $\text{MnCo}_2\text{O}_4$ . To keep the spinel structure, the Mn atoms occupy the  $\text{Co}^{\text{III}}$ 's sites, so the Mn presents dominant  $\text{Mn}^{\text{III}}$  in the bulk of  $\text{MnCo}_2\text{O}_4$ , which is consistent with the Mn XANES (Figure 2b) compared to  $\text{Mn}_2\text{O}_3$ ,  $\text{Mn}_3\text{O}_4$  and  $\text{MnO}_2$ .

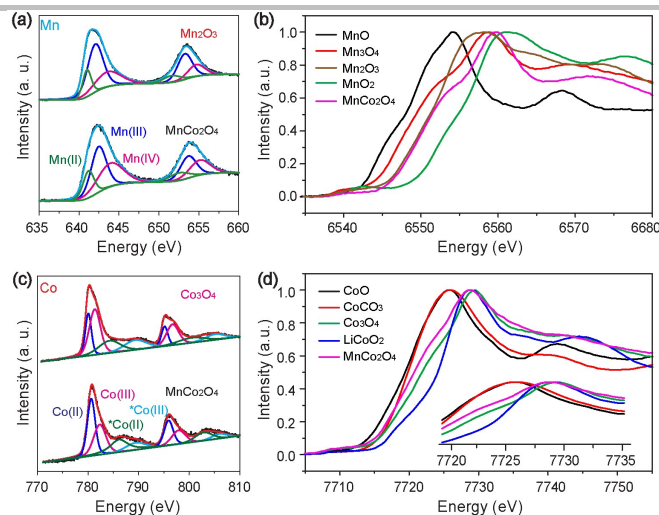


**Figure 2.** (a) Mn and (b) Co XPS spectra of  $\text{MnCo}_2\text{O}_4$ ,  $\text{Mn}_2\text{O}_3$  and  $\text{Co}_3\text{O}_4$ , (c) Mn and (d) Co K-edge XANES spectra of various samples. The inset of Figure 2d is the zoom map of XANES ranging from 7719 to 7735 eV.

To evaluate the property of  $\text{MnCo}_2\text{O}_4$  for OER, it was carried out in  $\text{O}_2$ -saturated 0.1 M KOH by polarization curves. As a comparison, a bare glassy carbon (GC) electrode, carbon (Vulcan XC-72), Pt/C (20 wt.% Pt),  $\text{Mn}_2\text{O}_3$ ,  $\text{Co}_3\text{O}_4$  and the physical mixture of  $\text{Mn}_2\text{O}_3$  and  $\text{Co}_3\text{O}_4$  were also performed under the same condition. From Figure 3a, the bare GC and carbon don't have a great effect on catalyzing OER. At  $10 \text{ mA cm}^{-2}$  (Figure 3b),  $\text{MnCo}_2\text{O}_4$  displays a small overpotential (0.40 V), which is comparable with  $\text{Co}_3\text{O}_4$  (0.39 V). The OER activity of Co-based spinel oxides relies on the relative ratio of  $\text{Co}^{\text{II}}/\text{Co}^{\text{III}}$ . Liu *et al.* found that  $\text{Co}^{\text{II}}$  is beneficial for forming cobalt oxyhydroxide ( $\text{CoOOH}$ ), which is responsible for enhanced OER.<sup>[12]</sup> In contrast,  $\text{Co}^{\text{III}}$  tends to improve the strength between catalysts' surface and hydroxides groups, which lowers the activity of OER. It is fortunate that the as-synthesized  $\text{MnCo}_2\text{O}_4$  possesses dominant  $\text{Co}^{\text{II}}$  in the both surface and bulk, causing the highly-comparable OER activity to  $\text{Co}_3\text{O}_4$ . In addition, the OER activity for the physical mixture of  $\text{Mn}_2\text{O}_3$  and  $\text{Co}_3\text{O}_4$  is less active than  $\text{MnCo}_2\text{O}_4$ , which indicates the importance of the chemical synergic coupling of Mn and Co to enhance the electrochemical activity. Taking account of surface area and catalyst loading, the specific activity ( $j_s$ ) and mass activity ( $j_m$ ) were also used to compare OER activity of catalysts (Table S2). It is shown that the specific activity and mass activity of  $\text{MnCo}_2\text{O}_4$  ( $j_s$ :  $20.60 \text{ mA g}^{-1}$ ,  $j_m$ :  $90 \text{ } \mu\text{A cm}^{-2}$ ) are as good as that of  $\text{Co}_3\text{O}_4$  ( $j_s$ :  $22.90 \text{ mA g}^{-1}$ ,  $j_m$ :  $110 \text{ } \mu\text{A cm}^{-2}$ ).

From Figure 3c, we can find that the Tafel slope of  $\text{MnCo}_2\text{O}_4$  is  $90 \text{ mV decade}^{-1}$ , which is slightly higher than  $\text{Co}_3\text{O}_4$  ( $71 \text{ mV decade}^{-1}$ ) and lower than the physical mixture of  $\text{Mn}_2\text{O}_3$  and  $\text{Co}_3\text{O}_4$ . A lower Tafel slope means the relevant material can favor the kinetic of OER, which indicates that  $\text{MnCo}_2\text{O}_4$  has a great OER activity.<sup>[13]</sup> Charge transport is a crucial factor for the kinetics of OER.<sup>[14]</sup> Electrochemical impedance spectroscopy (EIS) was used to study the charge rate of catalysts (Figure S3).



## COMMUNICATION

WILEY-VCH

The charge transfer resistance ( $R_{ct}$ ) follows the order of Pt/C >  $Mn_2O_3$  > the physical mixture of  $Mn_2O_3$  and  $Co_3O_4$  >  $MnCo_2O_4$  >  $Co_3O_4$ , which is associated with their OER activities.

Cyclic voltammetry (CV) was used to assess the ORR electrocatalytic properties of  $MnCo_2O_4$ . From the Figure 3d, the peak potential of  $MnCo_2O_4$  appears at 0.83 V, which provides a similar ORR activity with  $Mn_2O_3$  (0.85 V) and Pt/C (0.87 V). The peak potential of  $MnCo_2O_4$  is slightly negative to  $Mn_2O_3$ . There are two reasons causing this gap. Firstly, by comparison with  $Mn^{III}$  and  $Mn^{IV}$ , Co-based species don't have a great effect on the enhancement of ORR. Secondly,  $Mn_2O_3$  has a larger surface area than  $MnCo_2O_4$ . Compared with  $Co_3O_4$  (peak potential: 0.69 V) the high ORR activity of  $MnCo_2O_4$  can be attributed to the substitution of Mn.  $Mn^{III}$  and  $Mn^{IV}$  are more active ORR sites than Co-based species.<sup>[15]</sup> On one hand, the presence of  $Mn^{III}$  can promote the ORR kinetics.<sup>[16]</sup> On the other hand, the amount of peroxide can be decomposed by  $Mn^{IV}$ . The physical mixture of  $Mn_2O_3$  and  $Co_3O_4$  (peak potential: 0.78 V) offers lower ORR activity than  $MnCo_2O_4$ , suggesting that chemical synergistic effect also has a great advantage in the enhancement of ORR.

Rotating disk electrode (RDE) was employed to gain insight into the ORR kinetic of catalysts. The onset potential of  $MnCo_2O_4$  is 0.95 V (Figure 3e and S4), which can be comparable with  $Mn_2O_3$  (0.98 V) and Pt/C (1.00 V). In addition, the limiting current of  $MnCo_2O_4$  is close to Pt/C. The electron transfer number ( $n$ ) was calculated from polarization curves according to the Koutecky-Levich (K-L) equation (Figure 3f). It is well known that Pt/C follows a 4e transfer mechanism.<sup>[17]</sup> According to K-L equation, the electron transfer number of  $MnCo_2O_4$  was calculated to be 3.94, which approaches that of  $Mn_2O_3$  (3.97). Considering the contribution of catalysts' mass and specific surface area to ORR, mass activity and specific activity of catalysts were measured. From Table S3, the mass activity and specific activity of  $MnCo_2O_4$  ( $j_s$ : 0.83 mA g<sup>-1</sup>;  $j_m$ : 30  $\mu$ A cm<sup>-2</sup>) is larger than  $Co_3O_4$  ( $j_s$ : 0.21 mA g<sup>-1</sup>;  $j_m$ : 10  $\mu$ A cm<sup>-2</sup>). The incorporation of  $Mn^{III}/Mn^{IV}$  in  $Co_3O_4$  forms  $MnCo_2O_4$ , leading to the decrement of peroxide and the increment of the electron transfer number. Consequently, the sluggish kinetic of ORR would be facilitated.

Rotating ring-disk electrode (RRDE) was used to explore the electron transfer number and the peroxide yield of  $MnCo_2O_4$  (Figure S5).  $MnCo_2O_4$  shows a high disk current for the reduction of  $O_2$  and a low ring current for the oxidation of peroxide. The peroxide yield of  $MnCo_2O_4$  fluctuates between 4 % and 6 % over the potential from 0.4 V to 0.7 V (Figure 4a), which is similar to that of  $Mn_2O_3$  and less than the reported  $MnCo_2O_4$ /N-rmGO (nearly 10%).<sup>[11]</sup> For  $Co_3O_4$ , the  $n$  value is lower than  $MnCo_2O_4$  and the peroxide yield reaches 35 %, indicating that oxygen was mainly reduced to peroxide. RRDE confirms that  $MnCo_2O_4$  shows a great excellent activity toward ORR, which is aligned with

RDE results. The oxygen strength on metal oxides' surface is a key step of ORR. The oxygen strength will be decreased by the reaction of  $Mn^{IV}/Mn^{III}$ , resulting to the acceleration of the kinetics of ORR.<sup>[7a]</sup> The smaller amount of peroxide generated on  $MnCo_2O_4$ 's surface should be originated from the coexistence of  $Mn^{III}/Mn^{IV}$ . The introduction of  $Mn^{III}$  and  $Mn^{IV}$  in  $Co_3O_4$  forming  $MnCo_2O_4$  makes great contributions to increasing the electron number of ORR. The long-term stability of  $MnCo_2O_4$  was studied by chronoamperometric measurements. After 10 h, the loss of current density for  $MnCo_2O_4$  is only 15 % (Figure 4b), indicating high stability of  $MnCo_2O_4$  than Pt/C.

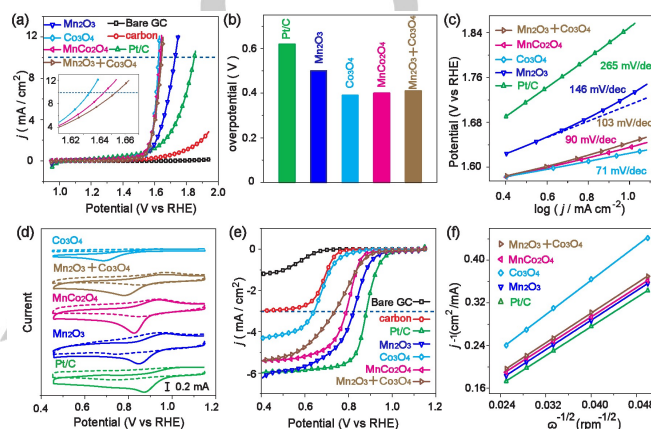


**Figure 3.** (a) OER polarization curves of catalysts at 1600 rpm; (b) Overpotentials derived from OER polarization curves at  $j=10$  mA cm<sup>-2</sup>; (c) Tafel plots derived from OER polarization curves; (d) CV of catalysts; (e) ORR polarization curves of catalysts at 1600 rpm; (f) K-L plots of catalysts. All measurements were performed in  $O_2$ -saturated 0.1 M KOH.

To quantitatively evaluate the bifunctional oxygen electrode activity of  $MnCo_2O_4$ , a metric was adopted and used to compare the difference between the ORR potential at -3 mA cm<sup>-2</sup> and the OER potential at 10 mA cm<sup>-2</sup>. The smaller the potential difference, the better the catalyst's bifunctional activity is. The potential difference between ORR metric and OER metric of  $MnCo_2O_4$  is only 0.83 V (Table S4), which can be comparable with the most excellent reported N, P-GCNs (0.71 V). The unique surface state of Mn and Co is the source to the high performance. The dominant surface  $Mn^{IV}$  gives birth to excellent ORR activity while superior surface  $Co^{II}$  contributes efficient OER performance. To determine this claiming, the bifunctional oxygen catalysis of  $H_2$ -treated  $MnCo_2O_4$  samples was investigated. As shown in Figure S6a and b, the performance decreased after  $H_2$ -treatment at both 200 °C and 400 °C, and ORR activity inhibition appears much more dominant. Based on the XANES spectra of  $H_2$ -treated  $MnCo_2O_4$  samples (Figure S6c and d) at 200 °C, we can find that the bulk structure maintains well compared to that of fresh  $MnCo_2O_4$  sample. However, the OER and ORR activity presents notable difference, indicating that the structure change happens in the surface. Furthermore, after  $H_2$ -treatment at 400 °C, the bulk structure changes apparently, where the binding

## COMMUNICATION

WILEY-VCH

energy of Co moves to CoO and the Mn shifts toward  $\text{Mn}_3\text{O}_4$ . While, the activity toward both OER and ORR differs very slightly from that of  $\text{MnCo}_2\text{O}_4$ -H200 sample, suggesting that the contribution of bulk structure is much less dominant compared to the surface state.

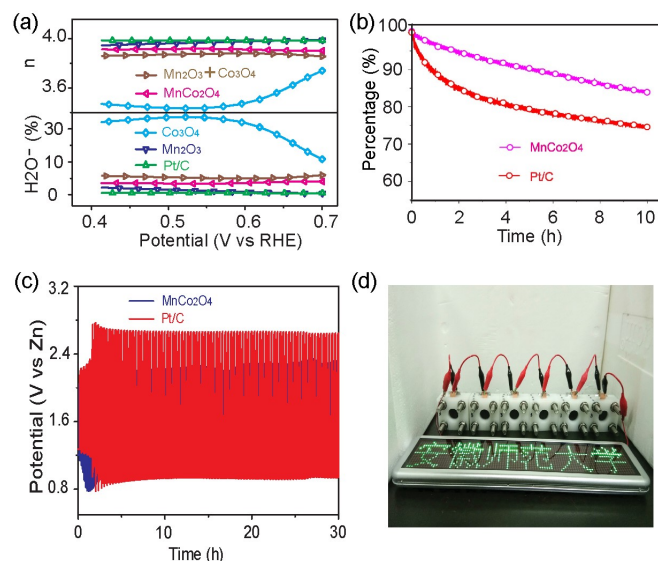


**Figure 4.** (a) Percentage of peroxide and electron numbers ( $n$ ) of  $\text{Co}_3\text{O}_4$ ,  $\text{Mn}_2\text{O}_3$ ,  $\text{MnCo}_2\text{O}_4$ , Pt/C and the physical mixture of  $\text{Mn}_2\text{O}_3$  and  $\text{Co}_3\text{O}_4$ . (b) Chronoamperometric measurements of  $\text{MnCo}_2\text{O}_4$  and Pt/C measured at -0.3 V (V vs Ag/AgCl) in  $\text{O}_2$ -saturated 0.1 M KOH at 1600 rpm. (c) Discharge-charge cycling curves at 10  $\text{mA}/\text{cm}^2$  of rechargeable Zn-air batteries with  $\text{MnCo}_2\text{O}_4$  and Pt/C; (d) A green LED panel powered by six Zn-air batteries ( $\text{MnCo}_2\text{O}_4$ ).

A home-build Zn-air battery was used to study the bifunctional stability of  $\text{MnCo}_2\text{O}_4$  (Figure 4d). The stability was performed by the discharge-charge cycling in 0.2 M  $\text{Zn}(\text{CH}_3\text{COO})_2$  and 6.0 M KOH. The discharge-charge curves were examined at 10  $\text{mA}/\text{cm}^2$  (Figure 4c). The initial discharge and charge potential of  $\text{MnCo}_2\text{O}_4$  are respectively 1.21 V and 2.05 V. After 180 cycles, there is small potential change in discharge (1.10 V) and charge (2.32 V). Although Pt/C has a high potential (1.27 V) during discharge process at first, the stable discharge potential of Pt/C is only ~0.88 V. This result shows that the stability of  $\text{MnCo}_2\text{O}_4$  is still excellent during the practical application.

In summary, a mesoporous  $\text{MnCo}_2\text{O}_4$  bifunctional oxygen electrocatalyst was synthesized by spray-pyrolysis route. The product possesses a remarkably high activity toward both OER and ORR. The unique  $\text{Mn}^{\text{IV}}$  and  $\text{Co}^{\text{II}}$ -rich surface state is the source to the high OER and ORR activity. It makes possible that  $\text{MnCo}_2\text{O}_4$  has the potential of being applied to promote the development of renewable energy technologies and devices. Additionally, the products produced through spray-pyrolysis can be sustainably obtained in a large scale with the precise components. The surface state engineering through modulating the chemical state of elements opens up attractive opportunities to synthesize a large number of new materials with excellent performance.

## Acknowledgments

This work was supported by the National Natural Science Foundation of China (21471006, 21271009), the Recruitment Program for Leading Talent Team of Anhui Province, the Program for Innovative Research Team of Anhui Education Committee, and the Research Foundation for Science and Technology Leaders and Candidates of Anhui Province.

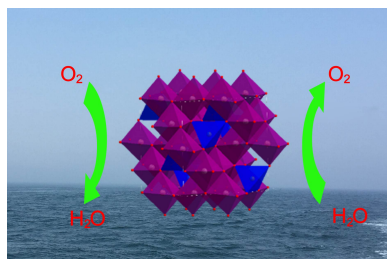
**Keywords:**  $\text{MnCo}_2\text{O}_4$  • mesoporous • mass production • surface state • bifunctional oxygen electrocatalysis

- [1] a) Z. H. Zhao, M. T. Li, L. P. Zhang, L. M. Dai, Z. H. Xia, *Adv. Mater.* **2015**, 27, 6834; b) H. F. Wang, C. Tang, B. Wang, B. Q. Li, Q. Zhang, *Adv. Mater.* **2017**, DOI: 10.1002/adma.201702327.
- [2] a) X. Q. Huang, Z. P. Zhao, L. Cao, Y. Chen, E. B. Zhu, Z. Y. Lin, M. F. Li, A. M. Yan, A. Zettl, Y. M. Wang, X. F. Duan, T. Mueller, Y. Huang, *Science* **2015**, 348, 1230; b) F. Calle-Vallejo, J. Tymoczko, V. Colic, Q. H. Vu, M. D. Pohl, K. Morgenstern, D. Loffreda, P. Sautet, W. Schuhmann, A. S. Bandarenka, *Science* **2015**, 350, 185.
- [3] a) J. W. Ren, M. Antonietti, T.-P. Feller, *Adv. Energy Mater.* **2015**, 5, 1401660; b) M. Gorlin, P. Chernev, J. Ferreira de Araujo, T. Reier, S. Dresch, B. Paul, R. Krahnert, H. Dau, P. Strasser, *J. Am. Chem. Soc.* **2016**, 138, 5603; c) Y. L. Zhu, W. Zhou, J. Sunarso, Y. J. Zhong, Z. P. Shao, *Adv. Funct. Mater.* **2016**, 30, 1501000.
- [4] M. Escudero-Escribano, P. Malacrida, M. H. Hansen, U. G. Vej-Hansen, A. Velazquez-Palenzuela, V. Tripkovic, J. Schiøtz, J. Rossmeisl, I. E. L. Stephens, I. Chorkendorff, *Science* **2016**, 352, 73.
- [5] a) D. J. Chen, C. Chen, Z. M. Baiyee, Z. P. Shao, F. Ciucci, *Chem. Rev.* **2015**, 115, 9869-9921; b) Y. G. Li, H. J. Dai, *Chem. Soc. Rev.* **2014**, 43, 5257-5275; c) G. L. Tian, M. Q. Zhao, D. S. Yu, X. Y. Kong, J. Q. Huang, Q. Zhang, F. Wei, *Small* **2014**, 10, 2251; d) R. Li, Z. D. Wei, X. L. Gou, *ACS Catal.* **2015**, 5, 4133; e) J. T. Zhang, Z. H. Zhao, Z. H. Xia, L. M. Dai, *Nat. Nanotechnol.* **2015**, 10, 444.
- [6] a) Y. Y. Zhao, C. Chang, F. Teng, Y. Y. Zhao, G. B. Chen, R. Shi, G. I. N. Waterhouse, W. F. Huang, T. R. Zhang, *Adv. Energy Mater.* **2017**, DOI: 10.1002/aenm.201700005. b) C. X. Guo, Y. Zheng, J. R. Ran, F. X. Xie, M. Jaroniec, S. Z. Qiao, *Angew. Chem. Int. Ed.* **2017**, 56, 8539; *Angew. Chem.* **2017**, 129, 8659.
- [7] a) J. Suntivich, H. A. Gasteiger, N. Yabuuchi, H. Nakanishi, J. B. Goodenough, Y. Shao-Horn, *Nat. Chem.* **2011**, 3, 546; b) K. Lei, X. Han, Y. Hu, X. Liu, L. Cong, F. Cheng, J. Chen, *Chem. Commun.* **2015**, 51, 11599. c) K. A. Stoerzinger, M. Risch, B. Han, Y. Shao-Horn, *ACS Catal.* **2015**, 5, 6021. d) H. Hu, B. Y. Guan, B. Y. Xia, X. W. Lou, *J. Am. Chem. Soc.* **2015**, 137, 5590.
- [8] a) P. W. Menezes, A. Indra, N. R. Sahraie, A. Bergmann, P. Strasser, M. Driess, *ChemSusChem* **2015**, 8, 164. b) X. C. Cao, J. Wu, C. Jin, J. H. Tian, P. Strasser, R. Z. Yang, *ACS Catal.* **2015**, 5, 4890; c) J. F. Li, S. L. Xiong, X. W. Li, Y. T. Qian, *Nanoscale* **2013**, 5, 2045.
- [9] W. H. Wang, J. Geng, L. Kuai, M. Li, B. Y. Geng, *Chem. Eur. J.* **2016**, 22, 9909.
- [10] a) L. Kuai, J. Geng, C. Y. Chen, E. J. Kan, Y. D. Liu, Q. Wang, B. Y. Geng, *Angew. Chem. Int. Ed.* **2014**, 53, 7547; b) L. Kuai, J. F. Wang, T. Ming, C. H. Fang, Z. H. Sun, B. Y. Geng, J. F. Wang, *Sci. Rep.* **2015**, 5, 9923.
- [11] Y. Y. Liang, H. L. Wang, J. G. Zhou, Y. G. Li, J. Wang, T. Regier, H. J. Dai, *J. Am. Chem. Soc.* **2012**, 134, 3517.
- [12] a) H. Y. Wang, S. F. Hung, H. Y. Chen, T. S. Chan, H. M. Chen, B. Liu, *J. Am. Chem. Soc.* **2016**, 138, 36. b) Y. Y. Liang, Y. G. Li, H. L. Wang, H. J. Dai, *J. Am. Chem. Soc.* **2013**, 135, 2013.
- [13] X. Liu, M. Park, M. G. Kim, S. Gupta, G. Wu, J. Cho, *Angew. Chem. Int. Ed.* **2015**, 54, 9654.
- [14] a) Y. T. Meng, W. Q. Song, H. Huang, Z. Ren, S. Y. Chen, S. L. Suib, *J. Am. Chem. Soc.* **2014**, 136, 11452. b) T. Y. Ma, S. Dai, M. Jaroniec, S. Z. Qiao, *J. Am. Chem. Soc.* **2014**, 136, 13925.
- [15] M. H. Shao, Q. W. Chang, J. P. Dodelet, R. Chenitz, *Chem. Rev.* **2016**, 116, 3594.
- [16] K. A. Stoerzinger, M. Risch, B. Han, Y. Shao-Horn, *ACS Catal.* **2015**, 5, 6021.
- [17] a) Y. L. Zhu, W. Zhou, R. Ran, Y. B. Chen, Z. P. Shao, M. L. Liu, *Nano Lett.* **2016**, 16, 512; b) D. Higgins, P. Zamani, A. P. Yu, Z. W. Chen, *Energy Environ. Sci.* **2016**, 9, 357.

Entry for the Table of Contents (Please choose one layout)

## COMMUNICATION

Mass-production of mesoporous  $\text{MnCo}_2\text{O}_4$  spinel with superior bifunctional  $\text{O}_2$  electrocatalysis is performed simply. The obtained  $\text{MnCo}_2\text{O}_4$  possesses dominant surface chemical state, which stimulate the excellent bifunctional performance.



Wenhai Wang, Long Kuai, Wei Cao,  
Marko Huttula, Sami Ollikkala, Taru  
Ahopelto, Ari-Pekka Honkanen, Simo  
Huotari, Mengkang Yu, Baoyou Geng\*

Page No. 1 – Page No. 6

Mass-production of Mesoporous  
 $\text{MnCo}_2\text{O}_4$  Spinel with  $\text{Mn}^{\text{IV}}$  and  $\text{Co}^{\text{II}}$ -  
rich Surface for Superior  
Bifunctional Oxygen Electrocatalysis